Synoptic Moisture Intrusion Provided Heavy Isotope Precipitations in Inland Antarctica during the Last Glacial Maximum

K. Kino[1], A. Cauquoin[2], A. Okazaki[3], T. Oki[1], and K. Yoshimura[2]

[1]Department of Civil Engineering, Graduate School of Engineering, the University of Tokyo, Tokyo, Japan

[2]Institute of Industrial Science, the University of Tokyo, Kashiwa, Japan

[3]Chiba University, Chiba, Japan

Corresponding author: Kanon Kino (kanon@hydra.t.u-tokyo.ac.jp)

Key Points:

- Synoptic circulations sustained the moisture transport toward inland Antarctica.
- Meridional sea surface temperature gradient enhanced moisture and heavy isotope precipitations on Antarctica, unlike sea ice expansion.
- Antarctic ice core isotopes may refine southern westerlies during the last glacial maximum.

Abstract

Stable water isotopes in inland Antarctic ice cores are powerful paleoclimate proxies; however, their relationship with dynamical atmospheric circulations remains controversial. Using a water isotope climate model (MIROC5-iso), we assessed the influence of the Last Glacial Maximum (LGM; ~21,000 years ago) sea surface temperatures (SST) and sea ice (SIC) on Antarctic precipitation isotopes ($\delta^{18}O_p$) through atmospheric circulation. The results revealed that the synoptic circulation mostly maintained southward moisture transport, reaching inland Antarctica. The steepened meridional SST gradient in the mid-latitudes increased $\delta^{18}O_p$ in inland Antarctica by enhancing the baroclinic instability and synoptic moisture transport. In contrast, enhanced SIC reduced the atmospheric humidity around Antarctica and lowered $\delta^{18}O_p$ through extensive surface cooling and transport from the ocean. These findings elucidate the isotopic proxies and enable us to constrain the southern hemisphere atmospheric circulation, including the westerlies, using ice cores during past climates, including the LGM.

Plain Language Summary

Stable water isotopes are widely used to reconstruct past variations of Earth's climate, such as the temperature in Antarctica during the Last Glacial Maximum (LGM) ~21,000 years ago. This is an essential period for the climate community, given the order of magnitude of the temperature change between the LGM and today, which is similar to that of today's warming. However, the relationship between stable water isotopes and temperature is still subject to debate because of the influence of other climatic factors. Using an isotope-enabled climate model, we found that the isotopic composition of Antarctic precipitation was not simply controlled by condensation temperature, but was substantially influenced by changes in dynamical atmospheric circulation related to sea surface temperature and sea ice expansion. We also suggest that representation of the past atmospheric circulations, including westerly jets, can be constrained using water isotopic signals in Antarctic ice cores.

1 Introduction

Ratios of stable isotopologues of water, $H_2{}^{16}O$, $H_2{}^{18}O$, and $HD^{16}O$, expressed hereafter in the usual δ notation (i.e., $\delta^{18}O$, with respect to V-SMOW scale; Dansgaard, 1964), from Antarctic ice cores have been widely used to study Earth's climate variations for the past several hundred thousand years. For example, the obtained $\delta^{18}O$ values allowed for describing the glacial-interglacial cycles over the past ~800,000 years (Augustin et al., 2004; Kawamura et al., 2017). The isotopic thermometer assumption, which regards the observed present-day spatial $T_a/\delta^{18}O$ slope as a surrogate for the temporal slope at a given site, has been classically used to reconstruct the mean surface air temperature changes (ΔT_a; Δ denotes changes between climates) in the past (Dahe et al., 1994; Dansgaard, 1964; Lorius et al., 1979; Lorius & Merlivat, 1977; Motoyama, 2005; Satow et al., 1999). Process-based reconstruction of the past Antarctic T_a was also carried out using simple one-dimensional Lagrangian isotope models or water isotope-enabled climate models (iso-GCMs). Still, there are considerable uncertainties in our understanding of the global and Antarctic climate and associated isotope changes during the last glacial maximum (LGM): an extremely cold climate period characterized by a low atmospheric CO_2 level (approximately 180 ppm) and highly extended ice-sheets in the northern hemisphere (NH) (Kageyama, Abe-Ouchi, et al., 2021). As for the global climate, the degree of global mean cooling (Kageyama, Harrison, et al., 2021), spatial sea surface conditions (Paul et al., 2021),

state of the ocean general circulation (Sherriff-Tadano & Klockmann, 2021), and the ice-sheet topographies (Ivanovic et al., 2016) are the major remaining issues. As for the processes determining $\delta^{18}O$ precipitation ($\delta^{18}O_p$) in Antarctica, the moisture origin (Uemura et al., 2018), sea ice extension (Lee et al., 2008), ice-sheet topography (Werner et al., 2018), surface inversion layer depth (Buizert et al., 2021), and precipitation seasonality (Erb et al., 2018) possibly affect the temporal $T_a/\delta^{18}O$ slope.

The role of atmospheric circulations in these processes has not been fully explored for past climates such as LGM despite extensive research. In modern Antarctica, several studies have indicated that dynamical circulations can influence $\delta^{18}O_p$ and temporal $T_a/\delta^{18}O_p$ slope (Dittmann et al., 2016; Fujita & Abe, 2006; Hirasawa et al., 2000, 2013; Kino et al., 2021; Noone & Simmonds, 2002; Schlosser et al., 2010, 2017; Stenni et al., 2016). Recent studies have also revealed the impacts of extreme precipitation events (EPE) on $\delta^{18}O_p$ in Antarctica (Dittmann et al., 2016; Kino et al., 2021; Schlosser et al., 2017; Servettaz et al., 2020). Typical EPEs, associated with synoptic circulations (including blocking events and atmospheric rivers), facilitate the intrusion of warm and humid air into Antarctica (Fujita & Abe, 2006; Hirasawa et al., 2000, 2013; Turner et al., 2019; Wang et al., 2023; Wille et al., 2021). Low-frequency (intra- to inter-seasonal) atmospheric variabilities, such as the Southern Annular Mode (SAM), also influence precipitation amounts (Marshall et al., 2017) and $\delta^{18}O_p$ in inland Antarctica (Kino et al., 2021). Such dynamical circulations could introduce bias to the $\delta^{18}O$ in Antarctic ice cores ($\delta^{18}O_{ice}$) as these ice cores are expected to reflect precipitation-weighted $\delta^{18}O_p$ (Krinner & Werner, 2003; Sime & Wolff, 2011; Werner et al., 2018). Southern mid-latitude atmospheric circulations, including the southern westerlies, are linked with sea surface temperature (SST) and sea ice concentration (SIC) in the mid-latitudes for both the present-day (Nakamura et al., 2008) and LGM (Sime et al., 2013) climates. Given the uncertainties of SST and SIC (Paul et al., 2021) and the southern westerlies (Kohfeld et al., 2013; Sime et al., 2013) during LGM, understanding key processes that change Antarctic $\delta^{18}O_p$ related to atmospheric circulations through a series of experiments for probable LGM conditions, is imperative.

In this study, the influence of southern mid-latitude atmospheric circulations on $\delta^{18}O_p$ in Antarctica during the past climate, namely LGM, was investigated in relation to SST and SIC. We applied two recent sea surface reconstructions (Paul et al., 2021; Sherriff-Tadano et al., 2023) as boundary conditions for an isotope-enabled atmospheric GCM (iso-AGCM). This approach allowed us to comprehensively investigate the influence of atmospheric circulation on the Antarctic $\delta^{18}O_p$. The remainder of this paper is organized as follows. In Section 2, the model, experimental settings, observational dataset, and analysis method are discussed. In Section 3, we evaluate the simulated LGM climates in Antarctica and analyze the processes ruling the $\delta^{18}O_p$ in Antarctica by investigating the differences between the simulated LGM experiments. In Section 4, we summarize our main findings concerning the combined effects of SST and SIC on $\delta^{18}O_p$ and discuss issues that need to be resolved.

2 Materials and Methods

2.1 Isotope-enabled atmospheric general circulation model

The atmospheric component of the fifth version of the Model for Interdisciplinary Research on Climate (MIROC; Watanabe et al., 2010) is based on a three-dimensional primitive equation in the hybrid σ–p coordinate, with spectral truncation adopted for horizontal discretization. Version MIROC5-iso, where water isotopes in the atmosphere and land surface

parts were implemented by Okazaki and Yoshimura (2017, 2019), was used in this study. The resolution of the MIROC5-iso was set to a horizontal spectral truncation of T42 (approximately 280 km) and 40 vertical layers. Okazaki and Yoshimura (2017, 2019) and Kino et al. (2021) discuss the detailed parameterizations of the models and their applications for global and Antarctic present-day conditions.

2.2 Experimental design

Four experiments were performed using MIROC5-iso (Table 1). A pre-industrial (PI) simulation was set up following the "piControl" experimental design in the Coupled Model Intercomparison Project-Phase 6 (CMIP6; Eyring et al., 2016). The mean SST and SIC fields (monthly averaged from 1870 to 1899) were obtained from the Atmospheric Modeling Intercomparison Project-Phase 2 (AMIP2; Taylor et al., 2000). Three LGM experiments were designed using the PMIP4 protocol (Kageyama et al., 2017). For the elevation and distribution of the ice-sheet, the GLAC-1D reconstruction at year 21 ka (Briggs et al., 2014; Ivanovic et al., 2016; Tarasov et al., 2012) was used. The land-sea mask was extended according to the ice-sheet. The boundary conditions of the land surface were the same as those in the PI simulation but masked by the LGM ice-sheet. The $\delta^{18}O$ of seawater was set to a globally uniform value (+1 ‰), according to Werner et al. (2018).

Table 1 Experimental designs in this study. NH and SH indicate the northern and southern hemispheres. M and G denote SIC provided by MIROC4m-AOGCM (Sherriff-Tadano et al., 2023) and GLOMAP (Paul et al., 2021), respectively.

Experimental name	Greenhouse gases & orbital parameters	Land surfaces		Ocean surfaces			
		Ice sheets & land-sea mask	others	SST	SIC in NH	SIC in SH	$\delta^{18}O_{sea\ water}$ [‰]
PI	PI	PI	PI	PI	PI	PI	0
LGM_G	LGM	LGM	PI	G	G	G	+1
LGM_M	LGM	LGM	PI	M	M	M	+1
LGM_Mw/Gice	LGM	LGM	PI	M	M	G	+1

The LGM simulations differ in the prescribed SST and SIC to force MIROC5-iso. Two recent sets were used to investigate the influence of sea surface conditions on LGM $\delta^{18}O_p$ in Antarctica. For LGM_G, the monthly SST and SIC provided by the Glacial Ocean MAP (GLOMAP; Paul et al., 2021) were used (Figure S1a). GLOMAP is a gridded LGM climatology reconstruction dataset based on faunal and floral assemblage data of the Multiproxy Approach for the Reconstruction of the Glacial Ocean Surface project and several estimates of the LGM SIC. GLOMAP exhibits higher cooling in the Southern Ocean (SO) than another reconstruction, as well as more extended SIC in this area. For LGM_M, SST and SIC simulated by Sherriff-Tadano et al. (2023; hereafter referred to as MIROC) were used (Figure S1b). The fourth generation of MIROC atmosphere-ocean GCM simulated the weak Atlantic meridional overturning circulation during LGM suggested by proxies, resulting in warmer LGM SST in the SO than in the other models (Sherriff-Tadano et al., 2023). Sherriff-Tadano et al. (2023) further improved expressions of mixed-phased clouds and reduced surface warm biases in the SO. Detailed setup of MIROC5-iso simulations are presented in Text S1.

The sensitivity experiment, LGM_Mw/Gice (i.e., MIROC SST and GLOMAP SIC), was conducted to determine the effects of SST and SIC that differed from those of LGM_G and LGM_M. Therefore, LGM_G minus LGM_Mw/Gice (LGM_Mw/Gice minus LGM_M) indicates the individual influence of changes in SST (SIC). The SST and SIC changes between LGM experiments are shown in Figures 1a–b and 2e–f.

2.3 Proxy data for model evaluation

Ten Antarctic ice core records were used for evaluation. For EDML, Dome B, Vostok, Dome C, Taylor Dome, Talos, WDC, and Byrd, $\Delta\delta^{18}O_{ice}$ and ΔT_a for LGM minus PI in LGM compiled by Werner et al. (2018) was employed. For $\Delta\delta^{18}O$ of the South Pole, we used the results of Steig et al. (2021). Each site location is shown in Figure 2a.

$\Delta\delta^{18}O$ data from speleothems (Comas-Bru et al., 2019; 2020) and ice cores (Kawamura et al., 2007; Landais et al., 2013; Uemura et al., 2018) were used to evaluate the simulated LGM climates at the global scale. For speleothems, $\Delta\delta^{18}O$ in the calcite was obtained from the Speleothem Isotope Synthesis and Analysis version 2 (SISALv2) dataset (Comas-Bru et al., 2019). The speleothem values of $\Delta\delta^{18}O$ were converted in drip water as performed by Cauquoin et al. (2019), using the respective experiments and method outlined by Tremaine et al. (2011).

2.4 Analysis method

To investigate the impact of atmospheric variations across multiple timescales on moisture transport to Antarctica, we decoupled the contributions of synoptic (associated with EPEs), intra- to inter-seasonal (e.g., SAM), and climatological scale meridional moisture transports by following Newman et al. (2012). First, the climatological mean state was determined from daily time-series. The residuals of daily time-series anomalous from the daily climatology were further decoupled to low-frequency and synoptic. The low frequency was determined using a Lanczos low-pass filter, which passes periods greater than 10-day, and the residual represented periods less than 10-day (synoptic state) using the SciPy library. Such filtering methods were used for specific humidity (q) and meridional wind speed (v) in the model vertical layers. We finally obtained the vertically integrated moisture transport (Q) in each time scale as follows:

$$Q_m = \int_{p_s}^{0} \overline{p_s v_m q_m}\, dp/g,$$

$$Q_{LF} = \int_{p_s}^{0} \overline{p_s}\, \overline{v_{LF} q_{LF}} dp/g, \text{ and}$$

$$Q_{syn} = \int_{p_s}^{0} \overline{p_s}\, \overline{v_{syn} q_{syn}} dp/g.$$

Here, p_s is the surface pressure, and g is the gravity constant. The overbar represents the time mean, and the subscripts m, LF, and syn are the climatological mean, the low frequency, and the synoptic time scales, respectively.

3 Results

3.1 Evaluation of Last Glacial Maximum climate simulations in MIROC5-iso

By globally assessing the simulated $\delta^{18}O_p$ reduction from PI to LGM, we confirmed that MIROC5-iso reasonably reproduced the LGM climate with a root mean square error (RMSE) of ~ 3.1‰ between the modeled and observed $\Delta\delta^{18}O_p$ values (Figures S2b and S3b). Both LGM simulations showed polar amplification in NH and SH, as well as global surface cooling, which is consistent with previous studies (Cauquoin et al., 2023; Risi et al., 2010). The reproducibility in the mid-high and low latitudes varies based on the SST/SIC boundary conditions. The positive $\Delta\delta^{18}O_p$ in the tropics (+1–2 ‰) was significant in LGM_G simulation, resulting in a more optimized model-data agreement for tropical speleothems than in LGM_M simulation (Figures S2a and S3a).

For Antarctica, LGM_G and LGM_M results were reasonable compared to $\Delta\delta^{18}O_{ice}$ (Figure S4a). $\Delta\delta^{18}O_p$ in LGM_G and LGM_M exhibit different spatial distributions (Figures 2a–b). In the simulations, the respective $\Delta\delta^{18}O_p$ values of LGM_G and LGM_M were similar at Dome Fuji, South Pole, and Dome B and consistent with the $\Delta\delta^{18}O_{ice}$ at Dome Fuji and Dome B. The $\delta^{18}O$ reduction at South Pole was very underestimated in both LGM simulations, possibly because of the unrealistic reduction of mean precipitation related to the precipitation amount weighting effect on $\delta^{18}O_p$. The precipitation reduction from PI to LGMs was more at approximately 180˚ and less at 0˚ longitude (Figure S5). Such spatial distribution would be changed by the topography or local circulation. The LGM_M results were relatively more consistent with the $\Delta\delta^{18}O_{ice}$ than the LGM_G ones at EDML, Vostok, and Dome C, whereas LGM_G simulation overestimated the reduction for ~2‰ in these sites. In contrast, LGM_G values were in good agreement with the observed $\Delta\delta^{18}O_{ice}$ at WDC and Byrd, whereas LGM_M experiment underestimated the $\delta^{18}O$ reduction by ~3‰ in these sites. To resume, MIROC5-iso LGM_G and LGM_M simulations were generally in better agreement with isotopic observation in West and East Antarctica, respectively. For certain ice core sites, our $\Delta\delta^{18}O_p$ results differ from those of the LGM experiments by Cauquoin et al. (2023) carried out with ECHAM6-wiso. For example, the decrease in $\delta^{18}O_p$ at Dome C was larger than that at Dome Fuji in MIROC5-iso and the ice core records, whereas the opposite is modeled in ECHAM6-wiso. Despite the need to consider such inter-model discrepancies, our results are reasonable for discussing Antarctic $\delta^{18}O_p$ in the LGM.

In contrast to $\Delta\delta^{18}O_p$, simulated ΔT_a in LGM_G and LGM_M varied slightly (Figure S4b). Our simulation underestimated the cooling reconstructed from ice cores of EDML, Dome Fuji, Dome B, Vostok, and Dome C and overestimated that from Taylor Dome, Talos, WDC, and Byrd.

3.2 Role of the atmospheric circulation in determining $\Delta\delta^{18}O_p$ in interior Antarctica during the last glacial maximum

In this section, we discuss the processes contributing to $\delta^{18}O_p$ values in Antarctica in relation to the mid-latitude atmospheric circulations. Across PI and LGM experiments, the southward moisture transports were mostly maintained in Q_{syn}, followed by Q_{LF}, with minimal contribution from Q_m (Figure S6), consistent with the reanalysis data (Newman et al., 2012). Such results highlight the importance of understanding changes in Q_{syn} across the experiments to discuss the processes contributing to Antarctic $\delta^{18}O_p$. To this end, we decoupled the individual

effects of SST and SIC on the southern mid-high latitudes climate including Q_{syn} and Antarctic $\delta^{18}O_p$ by comparing LGM_Mw/Gice sensitivity experiments with LGM_G and LGM_M.

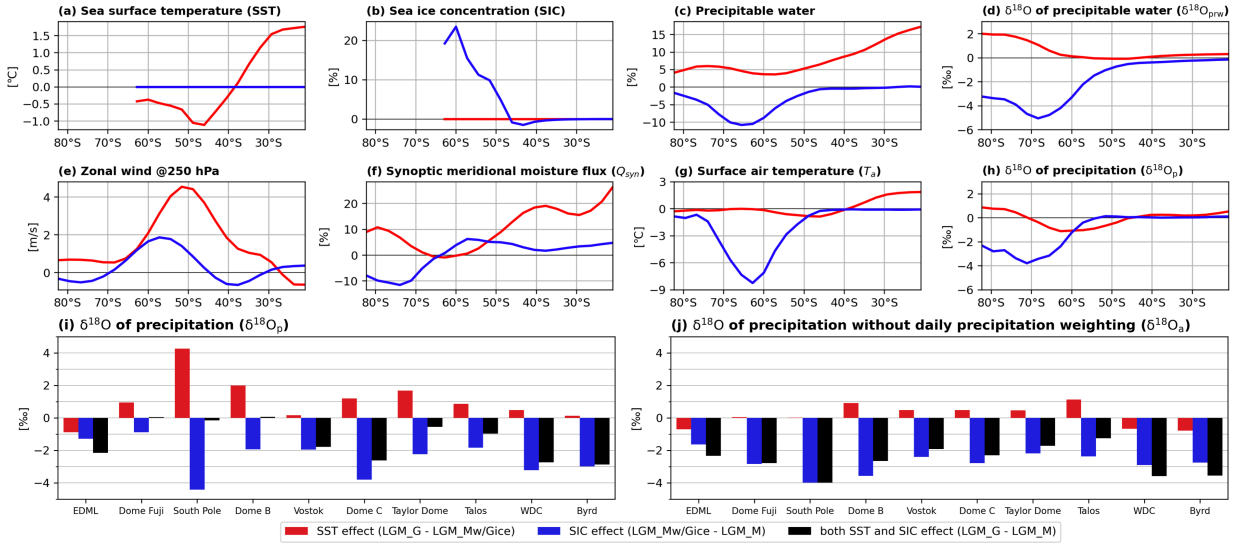

Figure 1 Sea surface temperature (SST) and sea ice (SIC) substitution impact the southern hemisphere climate. The red and blue curves and bars represent changes due to SST (from LGM_Mw/Gice to LGM_G) and SIC (from LGM_M to LGM_Mw/Gice). Zonal mean changes in **(a)** SST, **(b)** SIC, **(c)** precipitable water, **(d)** $\delta^{18}O$ of precipitable water ($\delta^{18}O_{prw}$), **(e)** zonal wind at 250hPa, **(f)** synoptic meridional moisture flux (Q_{syn}), **(g)** surface air temperature (T_a), **(h)** $\delta^{18}O$ of precipitation ($\delta^{18}O_p$). Changes in **(i)** $\delta^{18}O_p$ and **(j)** $\delta^{18}O_p$ without daily precipitation weighting ($\delta^{18}O_a$, see Text S2) at 10 Antarctic sites. For **(b), (c),** and **(f)**, changes are shown as ratios, while for the remaining panels, they are presented as anomalies. For **(e)** and **(f)**, the eastward and southward directions are indicated as positive, respectively. For **(i)** and **(j)**, changes due to the combination of both SST and SIC (from LGM_M to LGM_G) are also shown. Each site location is presented in Figure 2a.

3.2.1 SST substitution impacts (LGM_G minus LGM_Mw/Gice)

We investigated the effects of SST substitution from LGM_Mw/Gice to LGM_G in relation to the mid-latitude atmospheric circulation. The SST substitution warmed (cooled) SST at the north (south) of ~40°S (Figures 1a), increased (decreased) evaporation and sensible heat fluxes (Figures S7b–c). The increase in the Eady growth rate along the SST front (Figure S8), suggesting a stronger baroclinic instability, illustrates the role of the steepened meridional SST gradient (Figure S7a). These circulation changes enhanced the southward moisture fluxes, resulting from elevations in both humidity and southward winds (Figures S7f, 1c, and S7e).

The elevations in southward moisture fluxes described above predominantly occurred on the synoptic scale. The strengthened Q_{syn} by 5–10% increased the precipitable water by ~5% south of ~70°S (Figures 1f and 1c), resulting in an increase in the $\delta^{18}O$ of precipitable water ($\delta^{18}O_{prw}$) and $\delta^{18}O_p$ by ~2‰ and ~1‰, respectively, south of ~70°S (Figures 1d and 1h). The zonal mean Q_{LF} changed slightly south of ~70°S (Figure S7h). However, low-frequency variations in atmospheric circulation were not the primary factor but could indirectly influence the moisture fluxes through the synoptic circulations (Kino et al., 2021). The zonal mean Q_m

increased north of ~60°S, but not south of ~60°S (Figure S7g). The strengthened westerly jet (Figure 1e) was associated with the steepened meridional SST (Ogawa et al., 2016).

The spatially heterogeneous changes in $\Delta\delta^{18}O_p$ values in Antarctica (Figure 2c) can be partly attributed to the regional dominant atmospheric patterns (Kino et al., 2021; Marshall et al., 2017; Marshall & Thompson, 2016). Figure 2g shows an increase in the moisture inflow extended from the Ross Sea and West Antarctica, where the changes in sea level pressures and zonal winds were moderate (contours in Figures 2e and 2g), to East Antarctica. It suggests the importance of the southerly advection (Dittman et al., 2016; Schlosser et al., 2017) for moisture inflow. We analyzed the climatological $\delta^{18}O_p$ without daily precipitation weighting (hereafter referred to as $\delta^{18}O_a$, see Text S2) to evaluate the impacts of EPEs (Figure 1j). The small absolute values of $\Delta\delta^{18}O_a$ indicate that the effects of SST substitution were mostly related to EPEs. Moreover, the spatial heterogeneity of $\Delta\delta^{18}O_p$ minus $\Delta\delta^{18}O_a$ was pronounced (Figure S9a), indicating the contribution of the EPEs to $\Delta\delta^{18}O_p$ was uneven among sites. The southerly advection (Dittman et al., 2016; Schlosser et al., 2017) and various blocking patterns related to EPEs (Wang et al., 2023), along with variations in their occurrence frequency, would explain the relationship between EPEs and $\Delta\delta^{18}O_p$.

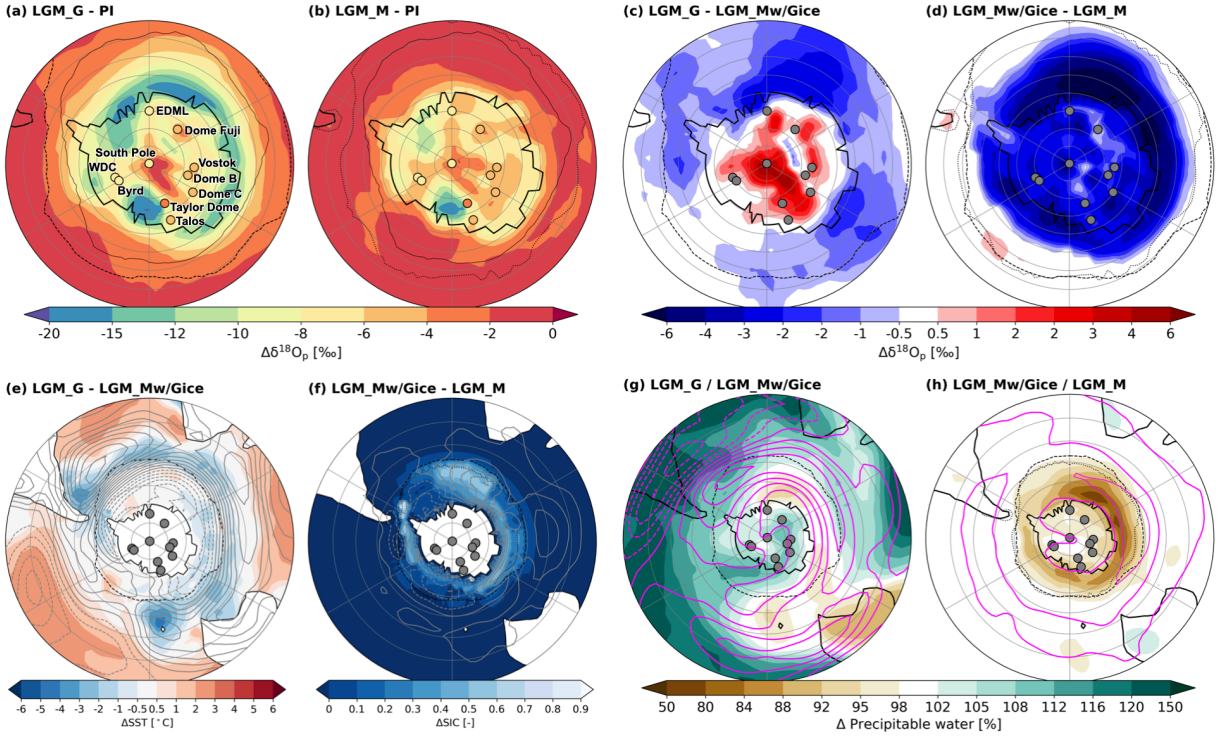

Figure 2 Climatological anomalies. **(a)** $\delta^{18}O$ of precipitation ($\delta^{18}O_p$) changes from Pre-Industrial (PI) to LGM_G in 50–90°S. **(b)** As in **(a)**, but for PI to LGM_M. **(c)–(d)** Changes due to sea surface temperature (SST) and sea ice concentration (SIC) substitutions: **(c)** from LGM_Mw/Gice to LGM_G; **(d)** from LGM_Mw/Gice to LGM_M. **(e)–(f)** As in **(c)–(d)**, but for SST and SIC, respectively, (shades) and sea level pressure (SLP; gray contours in every 0.5 hPa) in 20–90°S. **(g)–(h)** As in **(c)–(d)**, but for precipitable water (shades) and zonal winds at 250 hPa (magenta contours in every 2 m/s) in 20–90°S. For precipitable water in panels **(g)–(h)**, changes are presented as ratios, while for the remaining variables and panels, they are presented as anomalies. Positive anomalies for SLP and zonal winds are depicted with solid gray and magenta contours, respectively, while negative anomalies are dashed. Each panel denotes 15% SIC in PI, GLOMAP, and MIROC (thin solid, thick dashed, and thick dotted black contours, respectively). Each panel also denotes 10 Antarctic

ice core sites with circles; for **(a)**–**(b)**, these are overlaid with $\Delta\delta^{18}O_{ice}$. Refer to Section 2.2 for specifics on the sites.

3.2.2. SIC substitution impacts (LGM_Mw/Gice minus LGM_M)

We investigated the effects of SIC substitution from LGM_M to LGM_Mw/Gice, specifically SIC expansion in SH (Figure 1b), with respect to atmospheric circulation. In contrast to the SST substitution case, Q_{syn} decreased by ~10% and was partly compensated by Q_m south of ~70°S (Figures 1f and S7g). The precipitable water decreased by ~5% south of ~70°S and ~10% in 60–70°S, affected by strong cooling over SI (Figures 1c and 1g). The T_a reduction promoted isotopic fractionation during the transport from the open ocean to Antarctica. Combined with the extended transport pathway (Kohfeld et al., 2013; Sime et al., 2013, 2016), $\delta^{18}O_{prw}$ decreased extensively around Antarctica, resulting in $\delta^{18}O_p$ decreases by ~3 ‰ south of ~70°S (Figures 1d and 1h).

The reduction was strong in $\delta^{18}O_a$, too (Figure 1j), suggesting that the SIC substitution changed the mean isotopic environment around Antarctica and that EPEs were not the main controlling factor on $\delta^{18}O$ in precipitation. Nevertheless, the effects of SIC substitution on the EPEs were evidenced by the more pronounced variations in $\Delta\delta^{18}O_p$ than $\Delta\delta^{18}O_a$ among the sites (Figures 1i–j). The mean circulation changes due to the SIC substitution can explain such spatially uneven influences of EPEs. SIC anomaly between LGM_Mw/Gice and LGM_M was zonally non-uniform, particularly evident in the region in ~0–120°E (Figure 2f). This localized SIC expansion eased the stagnation of Rossby waves and reduced precipitable water (Figure 2h). Such blocking can influence oceanic inflows, thus affecting $\Delta\delta^{18}O_p$ minus $\Delta\delta^{18}O_a$ around Dome Fuji and Dome B (Figure S9).

4. Influence of sea surface conditions on southward moisture transport and $\delta^{18}O_p$ in inner Antarctica: discussion and perspectives

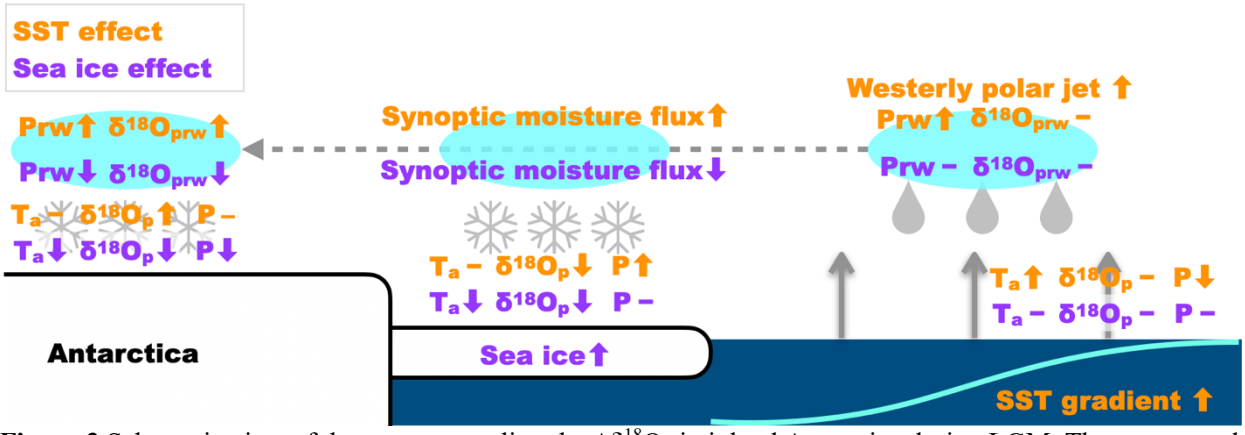

Figure 3 Schematic view of the processes ruling the $\Delta\delta^{18}O_p$ in inland Antarctica during LGM. The orange and purple colors represent the key processes associated with the substitution of SST (LGM_G minus LGM_Mw/Gice) and SIC (LGM_Mw/Gice minus LGM_M), respectively. The upward and downward arrows represent the increases and decreases of the values of the variables, respectively.

Our results revealed that the sea surface conditions influence southward moisture transport and $\delta^{18}O_p$ in inland Antarctica through synoptic circulations. Figure 3 illustrates the main findings of our study. To estimate these quantitative contributions, spatially heterogenous

$\Delta\delta^{18}O$ could be crucial. The impacts of the SST and SIC substitutions differed among sites, particularly with respect to EPEs. Appropriate sea surface conditions, atmospheric circulations, and Antarctic precipitation intensities are essential for adequately representing $\delta^{18}O_{ice}$ in iso-GCMs. Our three LGM experiments indicate that the synoptic circulations in the southern mid-latitudes, overlooked in studies utilizing the classical one-dimensional isotope model approach, are crucial in understanding $\delta^{18}O_p$ in inland Antarctica during the LGM. The spatial relationship of $\Delta\delta^{18}O_{ice}$ across Antarctic ice core sites could be a reliable indicator of these atmospheric circulations. Our study further suggests that investigating Antarctic ice cores with iso-GCMs can aid in more precisely constraining the behavior of LGM southern westerlies, which affect the SO circulation that traps atmospheric CO_2 in the deep ocean (Toggweiler et al., 2006).

Certain biases in MIROC5-iso and methodological limitations underscore the need for enhanced modeling to constrain LGM climate. MIROC5-iso overestimated summer precipitation intensity at Dome Fuji in the modern climate, possibly because of its low spatial resolution (Kino et al., 2021). Such bias would affect $\Delta\delta^{18}O_p$ and its relationship with ΔT_a and partly explain the spatial inconsistency between MIROC5-iso and ECHAM6-wiso in T63 (Cauquoin et al., 2023). Detailed comparisons among iso-GCMs are needed for more optimized constraints of the LGM climate. The westerly jets of the MIROC5 are biased equatorward in the modern climate (Watanabe et al., 2010). This bias may be associated with the features of westerlies and synoptic circulations in the LGM. Internal variability should also be discussed. The climatological $\delta^{18}O_p$ was determined by a combination of multiple moisture transport patterns, including blocking (Dittmann et al., 2016; Schlosser et al., 2017; Wang et al., 2023); 30-year analyses may be insufficient to evaluate the frequency of each pattern.

Further experiments forced by idealized SST and SIC (e.g., zonally uniform) will be performed to isolate and examine more precisely the impacts of SST gradients on atmospheric dynamics, leading to a better understanding of the mechanisms linking sea surface conditions to Antarctic $\delta^{18}O_p$. Evaluating d-excess profiles would also aid in establishing the connection between SST of the moisture source regions reconstructed from ice cores (Uemura et al., 2018) and the role of SST and SIC identified in this study. Further investigation is required to determine the effects of changes in ice-sheet elevation (Werner et al., 2018), precipitation seasonality (Erb et al., 2018), and the inversion layer depths (Buizert et al., 2021) on $\delta^{18}O_p$ in inland Antarctica. The global reproducibility of LGM climates is also important for more optimized Antarctic temperature estimations, as $\delta^{18}O_p$ in inland Antarctica is associated with the broader southern hemisphere. The two sets of LGM sea surface conditions used in this study were not the end members of PMIP models (Kageyama, Harrison, et al., 2021). Multiple LGM simulations would be required to constrain the LGM Antarctic temperatures.

Acknowledgments

- The first author was supported by the Japan Society for the Promotion of Science (JSPS) via a Grant-in-Aid for JSPS Fellows.
- This work was supported by the Japan Society for the Promotion of Science (JSPS) via Grants-in-Aid 17K14397, 19J14488, 21H05002, 22K14095, 22K21323, and JRPs-LEAD

with DFG via 416767181, and the Integrated Research Program for Advancing Climate Models (TOUGOU; JPMXD0717935457), ArCS II (JP-MXD1420318865), DIAS (JPMXD0716808979), and the advanced studies of climate change projection (SENTAN; JPMXD0722680395) from the Ministry of Education, Culture, Sports, Science and Technology (MEXT), Japan, and the Environment Research and Technology Development Fund S-20 (Grant Number JPMEERF21S12020) from the Environmental Restoration and Conservation Agency of Japan.

- We also thank Masakazu Yoshimori, Yukari Takayabu, Masahiro Watanabe, Hisashi Nakamura, Yukio Masumoto, Masahide Kimoto, Fumiaki Ogawa, and Satoru Okajima for their constructive comments.

Open Research

- Ice core data used for Figures S2 and S3 are available at https://www.ncdc.noaa.gov/data-access/paleoclimatology-data and are reported in Cauquoin et al. (2019). Ice core data used for Figures 1i and 2a–b, except for the South Pole, are available in Table 1 of Werner et al. (2018). Data for the South Pole is available at https://doi.org/10.15784/601239 (E. J. Steig et al., 2020). The SISAL speleothem dataset is available at https://doi.org/10.17864/1947.256 (Comas-Bru, Atsawawaranunt, et al., 2020). The GLOMAP is available at https://doi.pangaea.de/10.1594/PANGAEA.923262 (Paul et al., 2020). The SST and SIC outputs from MIROC4m-AOGCM are available from the authors of Sherriff-Tadano et al. (2023).

- The code of the isotopic version MIROC5-iso is available upon request on the IIS's GitLab repository (http://isotope.iis.u-tokyo.ac.jp:8000/gitlab/miroc-iso/miroc5-iso, Okazaki and Yoshimura, 2019).

- The source codes and data used in this study are available at https://github.com/kanonundgigue/kino2024grl and https://zenodo.org/doi/10.5281/zenodo.7582875 (Kino et al., 2024).

References

Augustin, L., Barbante, C., Barnes, P. R. F., Barnola, J. M., Bigler, M., Castellano, E., et al. (2004). Eight glacial cycles from an Antarctic ice core. *Nature*, *429*(6992), 623–628. https://doi.org/10.1038/nature02599

Augustin, L., Barbante, C., Barnes, P. R. F., Barnola, J. M., Bigler, M., Castellano, E., et al. (2004). Eight glacial cycles from an Antarctic ice core. *Nature*, *429*(6992), 623–628. https://doi.org/10.1038/nature02599

Ayako Abe-Ouchi, F. Saito, K. Kawamura, M. Raymo, J. Okuno, K. Takahashi, and H. Blatter: Insolation-driven 100,000-year glacial cycles and hysteresis of ice-sheet volume, *Nature, 500*, 190–193, 2013, doi:10.1038/nature12374

Briggs, R. D., Pollard, D., & Tarasov, L. (2014). A data-constrained large ensemble analysis of Antarctic evolution since the Eemian. *Quaternary Science Reviews, 103*, 91–115. https://doi.org/10.1016/j.quascirev.2014.09.003

Buizert, C., Fudge, T. J., Roberts, W. H. G., Steig, E. J., Sherriff-Tadano, S., Ritz, C., et al. (2021). Antarctic surface temperature and elevation during the Last Glacial Maximum. *Science, 372*(6546), 1097–1101. https://doi.org/10.1126/science.abd2897

Cauquoin, A., Abe-Ouchi, A., Obase, T., Chan, W.-L., Paul, A., & Werner, M. (2023). Effects of Last Glacial Maximum (LGM) sea surface temperature and sea ice extent on the isotope–temperature slope at polar ice core sites. *Climate of the Past, 19*(6), 1275–1294. https://doi.org/10.5194/cp-19-1275-2023

404 Cauquoin, A., Abe-Ouchi, A., Obase, T., Chan, W.-L., Paul, A., & Werner, M. (2023). Effects of
405 Last Glacial Maximum (LGM) sea surface temperature and sea ice extent on the isotope–
406 temperature slope at polar ice core sites. *Climate of the Past*, *19*(6), 1275–1294.
407 https://doi.org/10.5194/cp-19-1275-2023
408 Cauquoin, A., Risi, C., & Vignon, É. (2019). Importance of the advection scheme for the
409 simulation of water isotopes over Antarctica by atmospheric general circulation models: A
410 case study for present-day and Last Glacial Maximum with LMDZ-iso. *Earth and*
411 *Planetary Science Letters, 524*, 115731. https://doi.org/10.1016/j.epsl.2019.115731
412 Cauquoin, A., Werner, M., & Lohmann, G. (2019). Water isotopes – climate relationships for the
413 mid-Holocene and preindustrial period simulated with an isotope-enabled version of MPI-
414 ESM. *Climate of the Past, 15*(6), 1913–1937. https://doi.org/10.5194/cp-15-1913-2019
415 Comas-Bru, L., Atsawawaranunt, K., Harrison, S., & SISAL working group members. (2020).
416 SISAL (Speleothem Isotopes Synthesis and AnaLysis Working Group) database version
417 2.0 [Data set]. University of Reading. https://doi.org/10.17864/1947.256
418 Comas-Bru, L., Harrison, S. P., Werner, M., Rehfeld, K., Scroxton, N., Veiga-Pires, C., & SISAL
419 working group members. (2019). Evaluating model outputs using integrated global
420 speleothem records of climate change since the last glacial. *Climate of the Past, 15*(4),
421 1557–1579. https://doi.org/10.5194/cp-15-1557-2019
422 Comas-Bru, L., Rehfeld, K., Roesch, C., Amirnezhad-Mozhdehi, S., Harrison, S. P.,
423 Atsawawaranunt, K., et al. (2020, March 13). SISALv2: A comprehensive speleothem
424 isotope database with multiple age-depth models. *Earth System Science Data Discussions.*
425 https://doi.org/10.5194/essd-2020-39

426 Dahe, Q., Petit, J. R., Jouzel, J., & Stievenard, M. (1994). Distribution of stable isotopes in surface
427 snow along the route of the 1990 International Trans-Antarctica Expedition. *Journal of*
428 *Glaciology, 40*(134), 107–118. https://doi.org/10.3189/S0022143000003865
429 Dahe, Q., Petit, J. R., Jouzel, J., & Stievenard, M. (1994). Distribution of stable isotopes in surface
430 snow along the route of the 1990 International Trans-Antarctica Expedition. *Journal of*
431 *Glaciology*, *40*(134), 107–118. https://doi.org/10.3189/S0022143000003865
432 Dansgaard, W. (1964). Stable isotopes in precipitation. Tell'Us, 16(4), 436–468.
433 https://doi.org/10.3402/tellusa.v16i4.8993
434 Dittmann, A., Schlosser, E., Masson-Delmotte, V., Powers, J. G., Manning, K. W., Werner, M., &
435 Fujita, K. (2016). Precipitation regime and stable isotopes at Dome Fuji, East Antarctica.
436 *Atmospheric Chemistry and Physics, 16*(11), 6883–6900. https://doi.org/10.5194/acp-16-
437 6883-2016
438 Erb, M. P., Jackson, C. S., Broccoli, A. J., Lea, D. W., Valdes, P. J., Crucifix, M., & DiNezio, P.
439 N. (2018). Model evidence for a seasonal bias in Antarctic ice cores. *Nature*
440 *Communications, 9*(1), 1361. https://doi.org/10.1038/s41467-018-03800-0
441 Eyring, V., Bony, S., Meehl, G. A., Senior, C. A., Stevens, B., Stouffer, R. J., & Taylor, K. E.
442 (2016). Overview of the Coupled Model Intercomparison Project Phase 6 (CMIP6)
443 experimental design and organization. *Geoscientific Model Development, 9*(5), 1937–1958.
444 https://doi.org/10.5194/gmd-9-1937-2016
445 Fujita, K., & Abe, O. (2006). Stable isotopes in daily precipitation at Dome Fuji, East Antarctica.
446 *Geophysical Research Letters, 33*(18). https://doi.org/10.1029/2006GL026936

447 Hirasawa, N., Nakamura, H., & Yamanouchi, T. (2000). Abrupt changes in meteorological
448 conditions observed at an inland Antarctic Station in association with wintertime blocking.
449 *Geophysical Research Letters, 27*(13), 1911–1914. https://doi.org/10.1029/1999gl011039
450 Hirasawa, N., Nakamura, H., Motoyama, H., Hayashi, M., & Yamanouchi, T. (2013). The role of
451 synoptic-scale features and advection in prolonged warming and generation of different
452 forms of precipitation at Dome Fuji station, Antarctica, following a prominent blocking
453 event. *Journal of Geophysical Research, 118*(13), 6916–6928.
454 https://doi.org/10.1002/jgrd.50532
455 Ivanovic, Gregoire, Kageyama, Roche, Valdes, Burke, et al. (2016). Transient climate simulations
456 of the deglaciation 21--9 thousand years before present (version 1) -- PMIP4 Core
457 experiment design and boundary conditions. *Geoscientific Model Development, 9*(7),
458 2563–2587.
459 Kageyama, M., Abe-Ouchi, A., Obase, T., Ramstein, G., & Valdes, P. J. (2021). Modeling the
460 climate of the last glacial maximum from PMIP1 to PMIP4. In P. B. A. K. J. M. Paul J.
461 Valdes (Ed.) (Vol. 29, pp. 80–81). Past Global Changes (PAGES).
462 https://doi.org/10.22498/pages.29.2.80
463 Kageyama, M., Albani, S., Braconnot, P., Harrison, S. P., Hopcroft, P. O., Ivanovic, R. F., et al.
464 (2017). The PMIP4 contribution to CMIP6 -- Part 4: Scientific objectives and experimental
465 design of the PMIP4-CMIP6 Last Glacial Maximum experiments and PMIP4 sensitivity
466 experiments. *Geoscientific Model Development, 10*(11), 4035–4055. Retrieved from
467 https://gmd.copernicus.org/articles/10/4035/2017/
468 Kageyama, M., Harrison, S. P., Kapsch, M.-L., Lofverstrom, M., Lora, J. M., Mikolajewicz, U., et
469 al. (2021). The PMIP4 Last Glacial Maximum experiments: preliminary results and

comparison with the PMIP3 simulations. *Climate of the Past, 17*(3), 1065–1089. https://doi.org/10.5194/cp-17-1065-2021

Kawamura, K., Abe-Ouchi, A., Motoyama, H., Ageta, Y., Aoki, S., Azuma, N., et al. (2017). State dependence of climatic instability over the past 720,000 years from Antarctic ice cores and climate modeling. *Science Advances, 3*(2), e1600446. https://doi.org/10.1126/sciadv.1600446

Kawamura, K., Parrenin, F., Lisiecki, L., Uemura, R., Vimeux, F., Severinghaus, J. P., et al. (2007). Northern Hemisphere forcing of climatic cycles in Antarctica over the past 360,000 years. *Nature, 448*(7156), 912–916. https://doi.org/10.1038/nature06015

Kino, K., Okazaki, A., Cauquoin, A., & Yoshimura, K. (2021). Contribution of the southern annular mode to variations in water isotopes of daily precipitation at dome Fuji, east Antarctica. *Journal of Geophysical Research, 126*(23), e2021JD035397. https://doi.org/10.1029/2021jd035397

Kino, K., Okazaki, A., Cauquoin, A., & Yoshimura, K. (2021). Contribution of the southern annular mode to variations in water isotopes of daily precipitation at dome Fuji, east Antarctica. *Journal of Geophysical Research*, *126*(23). https://doi.org/10.1029/2021jd035397

Kohfeld, K. E., Graham, R. M., de Boer, A. M., Sime, L., Wolff, E. W., Le Quéré, C., & Bopp, L. (2013). Southern Hemisphere westerly wind changes during the Last Glacial Maximum: paleo-data synthesis. *Quaternary Science Reviews, 68*, 76–95. https://doi.org/10.1016/j.quascirev.2013.01.017

491 Krinner, G., & Werner, M. (2003). Impact of precipitation seasonality changes on isotopic signals
492 in polar ice cores: a multi-model analysis. *Earth and Planetary Science Letters, 216*(4),
493 525–538. https://doi.org/10.1016/S0012-821X(03)00550-8
494 Landais, A., Dreyfus, G., Capron, E., Jouzel, J., Masson-Delmotte, V., Roche, D. M., et al. (2013).
495 Two-phase change in CO2, Antarctic temperature and global climate during Termination
496 II. *Nature Geoscience, 6*(12), 1062–1065. https://doi.org/10.1038/ngeo1985
497 Lee, J.-E., Fung, I., DePaolo, D. J., & Otto-Bliesner, B. (2008). Water isotopes during the Last
498 Glacial Maximum: New general circulation model calculations. *Journal of Geophysical*
499 *Research, 113*(D19), 1341. https://doi.org/10.1029/2008JD009859
500 Lev Tarasov and W. Richard Peltier Greenland glacial history and local geodynamic
501 consequences, *Geophysical Journal International, 150*, July 2002, Pages 198-
502 229, doi:10.1046/j.1365-246X.2002.01702.x
503 Tarasov, L., Hughes, A., Gyllencreutz, R., Lohne, O.S., Mangerud, J., & Svendsen, J.I. The global
504 GLAC-1c deglaciation chronology, meltwater pulse 1-a, and a question of missing ice, IGS
505 Symposium on Contribution of Glaciers and Ice-sheets to Sea-Level Change, 2014
506 Lorius, C., & Merlivat, L. (1977). Distribution of mean surface stable isotope values in East
507 Antarctica, Isotopes and Impurities in Snow and Ice. *International Association of*
508 *Hydrological Sciences, Publication, 118*, 127–137.
509 Lorius, C., Merlivat, L., Jouzel, J., & Pourchet, M. (1979). A 30,000-yr isotope climatic record
510 from Antarctic ice. *Nature, 280*(5724), 644–648. https://doi.org/10.1038/280644a0
511 Marshall, G. J., & Thompson, D. W. J. (2016). The signatures of large-scale patterns of
512 atmospheric variability in Antarctic surface temperatures. *Journal of Geophysical*
513 *Research, 121*(7), 3276–3289. https://doi.org/10.1002/2015jd024665

514 Marshall, G. J., Thompson, D. W. J., & van den Broeke, M. R. (2017). The Signature of Southern
515 Hemisphere Atmospheric Circulation Patterns in Antarctic Precipitation. *Geophysical*
516 *Research Letters, 44*(22), 11580–11589. https://doi.org/10.1002/2017GL075998
517 Motoyama, H. (2005). Seasonal variations in oxygen isotope ratios of daily collected precipitation
518 and wind drift samples and in the final snow cover at Dome Fuji Station, Antarctica.
519 *Journal of Geophysical Research, 110*(D11). https://doi.org/10.1029/2004JD004953
520 Nakamura, H., Sampe, T., Goto, A., Ohfuchi, W., & Xie, S.-P. (2008). On the importance of
521 midlatitude oceanic frontal zones for the mean state and dominant variability in the
522 tropospheric circulation. *Geophysical Research Letters, 35*(15).
523 https://doi.org/10.1029/2008GL034010
524 Newman, M., Kiladis, G. N., Weickmann, K. M., Martin Ralph, F., & Sardeshmukh, P. D. (2012).
525 Relative Contributions of Synoptic and Low-Frequency Eddies to Time-Mean Atmospheric
526 Moisture Transport, Including the Role of Atmospheric Rivers. *Journal of Climate*, *25*(21),
527 7341–7361. https://doi.org/10.1175/JCLI-D-11-00665.1
528 Noone, D., & Simmonds, I. (2002). Annular variations in moisture transport mechanisms and the
529 abundance of δ18O in Antarctic snow. *Journal of Geophysical Research, 107*(D24), 4742.
530 https://doi.org/10.1029/2002JD002262
531 Ogawa, F., Nakamura, H., Nishii, K., Miyasaka, T., & Kuwano-Yoshida, A. (2016). Importance of
532 Midlatitude Oceanic Frontal Zones for the Annular Mode Variability: Interbasin
533 Differences in the Southern Annular Mode Signature. *Journal of Climate, 29*(17), 6179–
534 6199. https://doi.org/10.1175/JCLI-D-15-0885.1

535 Okazaki, A., & Yoshimura, K. (2017). Development and evaluation of a system of proxy data
536 assimilation for paleoclimate reconstruction. *Climate of the Past, 13*(4), 379–393.
537 https://doi.org/10.5194/cp-13-379-2017
538 Okazaki, A., & Yoshimura, K. (2019). Global evaluation of proxy system models for stable water
539 isotopes with realistic atmospheric forcing. *Journal of Geophysical Research, 124*(16),
540 8972–8993. https://doi.org/10.1029/2018jd029463
541 Paul, A., Mulitza, S., Stein, R., & Werner, M. (2020). Glacial Ocean Map (GLOMAP) [Data set].
542 PANGAEA. https://doi.org/10.1594/PANGAEA.923262
543 Paul, A., Mulitza, S., Stein, R., & Werner, M. (2021). A global climatology of the ocean surface
544 during the Last Glacial Maximum mapped on a regular grid (GLOMAP). *Climate of the*
545 *Past, 17*(2), 805–824. https://doi.org/10.5194/cp-17-805-2021
546 Risi, C., Bony, S., Vimeux, F., & Jouzel, J. (2010). Water-stable isotopes in the LMDZ4 general
547 circulation model: Model evaluation for present-day and past climates and applications to
548 climatic interpretations of tropical isotopic records. *Journal of Geophysical Research,*
549 *115*(D12), 108. https://doi.org/10.1029/2009jd013255
550 Satow, K., Watanabe, O., Shoji, H., & Motoyama, H. (1999). The relationship among
551 accumulation rate, stable isotope ratio and surface temperature on the plateau of east
552 Dronning Maud Land, Antarctica. *Polar Meteorology and Glaciology, 13*, 43–52.
553 https://doi.org/10.15094/00002888
554 Schlosser, E., Dittmann, A., Stenni, B., Powers, J. G., Manning, K. W., Masson-Delmotte, V., et
555 al. (2017). The influence of the synoptic regime on stable water isotopes in precipitation at
556 Dome C, East Antarctica. *The Cryosphere, 11*(5), 2345–2361. https://doi.org/10.5194/tc-
557 11-2345-2017

Schlosser, E., Manning, K. W., Powers, J. G., Duda, M. G., Birnbaum, G., & Fujita, K. (2010). Characteristics of high-precipitation events in Dronning Maud Land, Antarctica. *Journal of Geophysical Research, 115*(D14), 3518. https://doi.org/10.1029/2009JD013410

Servettaz, A. P. M., Orsi, A. J., Curran, M. A. J., Moy, A. D., Landais, A., Agosta, C., et al. (2020). Snowfall and water stable isotope variability in east Antarctica controlled by warm synoptic events. *Journal of Geophysical Research, 125*(17). https://doi.org/10.1029/2020jd032863

Sherriff-Tadano, S., & Klockmann, M. (2021). PMIP contributions to understanding the deep ocean circulation of the Last Glacial Maximum. *Past Global Change Magazine, 29*(2), 84–85. https://doi.org/10.22498/pages.29.2.84

Sherriff-Tadano, S., Abe-Ouchi, A., Yoshimori, M., Hotta, H., Kikuchi, M., Ohgaito, R., et al. (2023). Southern Ocean surface temperatures and cloud biases in climate models connected to the representation of glacial deep ocean circulation. *Journal of Climate*.

Sime, L., & Wolff, E. W. (2011, November 9). Antarctic accumulation seasonality. *Nature.* https://doi.org/10.1038/nature10613

Sime, L., Hodgson, D., Bracegirdle, T. J., Allen, C., Perren, B., Roberts, S., & de Boer, A. M. (2016). Sea ice led to poleward-shifted winds at the Last Glacial Maximum: the influence of state dependency on CMIP5 and PMIP3 models. *Climate of the Past, 12*(12), 2241–2253. https://doi.org/10.5194/cp-12-2241-2016

Sime, L., Kohfeld, K. E., Le Quéré, C., Wolff, E. W., de Boer, A. M., Graham, R. M., & Bopp, L. (2013). Southern Hemisphere westerly wind changes during the Last Glacial Maximum: model-data comparison. *Quaternary Science Reviews, 64*, 104–120. https://doi.org/10.1016/j.quascirev.2012.12.008

581 Steig, E. J., Jones, T. R., Kahle, E., Morris, V., Schauer, A., Vaughn, B., & White, J. (2020). South
582 Pole high resolution ice core water stable isotope record for dD, d18O [Data set]. South
583 Pole high resolution ice core water stable isotope record for dD, d18O. Antarctic Program
584 (USAP) Data Center. https://doi.org/10.15784/601239
585 Steig, Eric J., Jones, T. R., Schauer, A. J., Kahle, E. C., Morris, V. A., Vaughn, B. H., et al. (2021).
586 Continuous-Flow Analysis of δ17O, δ18O, and δD of H2O on an Ice Core from the South
587 Pole. *Frontiers of Earth Science in China, 9*, 72. https://doi.org/10.3389/feart.2021.640292
588 Stenni, B., Scarchilli, C., Masson-Delmotte, V., Schlosser, E., Ciardini, V., Dreossi, G., et al.
589 (2016). Three-year monitoring of stable isotopes of precipitation at Concordia Station, East
590 Antarctica. *The Cryosphere, 10*(5), 2415–2428. https://doi.org/10.5194/tc-10-2415-2016
591 Tarasov, L., Dyke, A. S., Neal, R. M., & Peltier, W. R. (2012). A data-calibrated distribution of
592 deglacial chronologies for the North American ice complex from glaciological modeling.
593 *Earth and Planetary Science Letters, 315–316*, 30–40.
594 https://doi.org/10.1016/j.epsl.2011.09.010
595 Taylor, K. E., Williamson, D., & Zwiers, F. (2000). The sea surface temperature and sea-ice
596 concentration boundary conditions for AMIP II simulations. Program for Climate Model
597 Diagnosis and Intercomparison, Lawrence River. Retrieved from
598 https://pcmdi.llnl.gov/report/pdf/60.pdf?id=16
599 Toggweiler, J. R., Russell, J. L., & Carson, S. R. (2006). Midlatitude westerlies, atmospheric CO2,
600 and climate change during the ice ages. *Paleoceanography, 21*(2).
601 https://doi.org/10.1029/2005PA001154
602 Tremaine, D. M., Froelich, P. N., & Wang, Y. (2011). Speleothem calcite farmed in situ: Modern
603 calibration of δ18O and δ13C paleoclimate proxies in a continuously-monitored natural

cave system. *Geochimica et Cosmochimica Acta, 75*(17), 4929–4950. https://doi.org/10.1016/j.gca.2011.06.005

Turner, J., Phillips, T., Thamban, M., Rahaman, W., Marshall, G. J., Wille, J. D., et al. (2019). The dominant role of extreme precipitation events in antarctic snowfall variability. *Geophysical Research Letters, 46*(6), 3502–3511. https://doi.org/10.1029/2018gl081517

Uemura, R., Motoyama, H., Masson-Delmotte, V., Jouzel, J., Kawamura, K., Goto-Azuma, K., et al. (2018). Asynchrony between Antarctic temperature and CO2 associated with obliquity over the past 720,000 years. *Nature Communications, 9*(1), 961. https://doi.org/10.1038/s41467-018-03328-3

Wang, S., Ding, M., Liu, G., Li, G., & Chen, W. (2023). Blocking Events in East Antarctica: Impact on Precipitation and Their Association with Large-scale Atmospheric Circulation Modes. *Journal of Climate, 1*(aop). https://doi.org/10.1175/JCLI-D-23-0419.1

Watanabe, M., Suzuki, T., O'ishi, R., Komuro, Y., Watanabe, S., Emori, S., et al. (2010). Improved Climate Simulation by MIROC5: Mean States, Variability, and Climate Sensitivity. *Journal of Climate, 23*(23), 6312–6335. https://doi.org/10.1175/2010JCLI3679.1

Werner, M., Jouzel, J., Masson-Delmotte, V., & Lohmann, G. (2018). Reconciling glacial Antarctic water stable isotopes with ice sheet topography and the isotopic paleothermometer. *Nature Communications, 9*(1), 3537. https://doi.org/10.1038/s41467-018-05430-y

Wille, J. D., Favier, V., Gorodetskaya, I. V., Agosta, C., Kittel, C., Beeman, J. C., et al. (2021). Antarctic atmospheric river climatology and precipitation impacts. *Journal of Geophysical Research, 126*(8). https://doi.org/10.1029/2020jd033788